ACS OMEGA

Open Access

http://pubs.acs.org/journal/acsodf

Article

Polyethylene Glycol Confined in SiO_2–Modified Expanded Graphite as Novel Form–Stable Phase Change Materials for Thermal Energy Storage

Giang Tien Nguyen,* Thi Ai Nhi Truong, Nguyen Duy Dat, Thi Anh Dao Phan, and Trung Huu Bui

Cite This: *ACS Omega* 2023, 8, 38160–38169

Read Online

ACCESS | Metrics & More | Article Recommendations

ABSTRACT: Form–stable phase change materials (FSPCMs) composed of poly(ethylene glycol) (PEG) encapsulated in SiO_2-modified expanded graphite (EG@SiO_2) were prepared and investigated for thermal energy storage behaviors. The modification of SiO_2 on EG was done using a simple sol–gel method, and then the resulting EG@SiO_2 was introduced to confine PEG at varying content (60–90 wt %). Surface properties (including microstructure, morphology, and functional groups), PEG adsorptivity, leakage-proof ability, and thermal energy storage of the prepared materials were thoroughly characterized and discussed. The EG@SiO_2 with 15 wt % SiO_2 outstandingly adsorbed PEG as compared to the pristine EG, showing up >80 wt % of PEG. As a result, PEG was well stabilized in EG@SiO_2 porous network without leakage, owing to capillary force, surface tension, and hydrogen bonding interactions. The optimal 80 wt % PEG/EG@SiO_2 composite possessed high crystallinity (93.5%), high thermal energy storage capacity (132.5 J/g), and excellent thermal conductivity (4.086 W/m·K). In addition, it exhibited good cycling durability after 500 repeated melting/crystallization cycles. The high thermal efficacy and inexpensiveness would make the PEG/EG@SiO_2 FSPCMs suitable for scale–up applications in thermal energy storage.

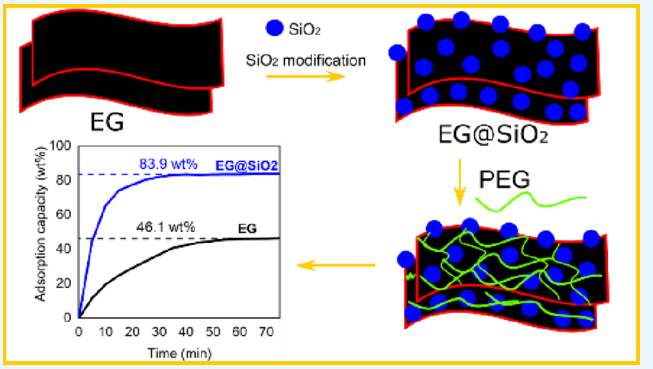

1. INTRODUCTION

Form–stable phase change materials (FSPCMs), also known as shape-stabilized phase change materials, consisting of phase change materials (PCMs) encapsulated in porous carriers, are thermal energy storage and conversion materials capable of reversibly storing and releasing large amounts of latent heat during solid–liquid phase transitions.[1] FSPCMs find extensive use in solar energy harvesting, building thermal management, hot/cold generation, waste heat recovery, and drug and food delivery, among other applications.[2−4] Within various FSPCMs, polyethylene glycol (PEG)-based ones have attracted significant attention due to low cost, high energy storage density, and high thermal cycling durability.[5,6] In this regard, porous carriers play a role as rigid scaffolds to confine and stabilize PCMs during phase transition, preventing them from liquid leakage. Various porous carriers, including SiO_2,[7,8] biomass porous carbon,[5] diatomite,[9] active carbon,[10] and $SrBaCO_3$,[6] have been studied for confining PEGs. PEGs encapsulated in SiO_2 exhibited good polar compatibility; however, a poor sustaining of crystallinity was often obtained due to interfacial hydrogen bonds with silanol (Si–OH) groups on the SiO_2 surface,[7,8] leading to poor thermal performance. Meanwhile, a low amount of PEG (50 wt %) was loaded in diatomite as reported somewhere.[9] Although the other carriers including biomass porous carbon, active carbon, and $SrBaCO_3$ showed good PEG adsorption capacities (80–86 wt %), the thermal conductivities of resulting FSPCMs could not be significantly improved because of the intrinsic low thermal conductivity of these substances.[5,6,10] Therefore, it is an art to select suitable porous carriers to effectively support PEGs and gain desirable thermophysical properties of FSPCMs.

Recently, expanded graphite (EG) has been extensively used as a low-cost porous carrier with exceptionally high thermal conductivity, adsorption capacity, and chemical stability.[11,12] Previous studies have shown that the incorporation of EG with PCMs such as *n*-eicosane,[12] stearic acid,[11] and tetradecanol[13] to form FSPCMs could enhance thermal conductivities of 14.4–20 times compared to those of pure PCMs. In terms of

Received: June 17, 2023
Accepted: September 21, 2023
Published: October 6, 2023

polarity, EG is hydrophobic due to its sp^2 carbon−carbon bonds, ketone bonds, and carbonyl bonds, making it compatible with less polar PCMs. Indeed, EG can easily adsorb and confine up to 80−90 wt % of PCMs like fatty acids,[11,14] paraffin waxes,[12,15] and fatty alcohols,[13] which are not greatly polar, thereby improving thermal performance. However, the combination of EG with hydrophilic PCMs presents challenges due to their polar incompatibility. During multiple cycles of solid−liquid phase transitions, hydrophilic PCMs may potentially seep out due to weak physical interactions with the porous carrier, leading to reduced cycling durability and service life.[16]

Modifying EG with suitable materials (e.g., surfactants and oxides) is a promising approach for enhancing the hydrophilicity of EG that is compatible with hydrophilic PCMs. For example, EG grafted with hydrophilic surfactants like OP−10[17] and TritonX−100[18] significantly enhanced the adsorption of hydrophilic PCMs, such as $CaCl_2{\cdot}6H_2O$ and MgCl2·6H2O-NH4Al(SO4)2·12H2O. However, the attachment of surfactants on EG surfaces is prone to be harmed because of poor interactions after repeated melting/crystallization cycles. Chen et al.[16] successfully modified EG surfaces with SiO_2, effectively increasing the hydrophilicity and compatibility of EG with a eutectic nitrate ($LiNO_3{\cdot}3H_2O$−KNO_3−$NaNO_3$). Zou et al.[19] reported that when EG surfaces was modified with TiO_2, $CaCl_2{\cdot}6H_2O$ could be easily dispersed and infiltrated into the EG structure. Gong et al.[20] used Al_2O_3−modified EG to support 1−octadecanol and found that the encapsulated 1−octadecanol exhibited high cycling durability after multiple phase change cycles. It is worth noting that the PCMs encapsulated in those oxide−modified EG materials demonstrated high adsorption (80−90 wt %) and high crystallinity (86.9−100%). Although these studies suggest a promising strategy for the effective fabrication of EG-based FSPCMs with polar PCMs, the limited number of studies hinders our understanding of the interfacial interactions toward polar organic PCMs, like PEGs. In this regard, PEGs have a long chain structure and high polar properties that may behave in distinct interactions with oxide and EG surfaces, affecting the crystallinity and thermal performance of this energy storage material.

SiO_2 is an inexpensive material with excellent hydrophilicity, high thermal and chemical stability, and nontoxicity. It could be used to modify EG surfaces by facile sol−gel methods,[16,21] making it suitable to tune EG surface properties. In this work, a series of SiO_2−modified expanded graphite (EG@SiO_2) porous carriers encapsulated with PEG PSPCMs were prepared and extensively investigated for thermal storage properties. The following subtopics were investigated: (1) preparation of EG@SiO_2 carrier using a simple sol−gel method, followed by loading a varying amount of PEG (60−90 wt %) to form PEG-based FSPCMs; (2) characterization of the prepared materials including the adsorptivity, microstructure, morphology, polar compatibility, and chemical compatibility; (3) determination of the thermal characteristics of PEG/EG@SiO_2 FSPCMs, including phase change enthalpy and temperature, crystallinity, leakage-proof ability, thermal stability, thermal conductivity, and cycling durability. Various instrumental analyses were performed for the investigation including scanning electron microscope (SEM), Fourier−transformed infrared spectroscopy (FTIR), differential scanning calorimetry (DSC), X-ray diffraction (XRD), thermogravimetric analysis, and transient plane source. The detailed data are shown and discussed in the manuscript.

2. RESULTS AND DISCUSSION

2.1. Characterization. Figure 1a−e exhibits the SEM images of the pristine EG and its modified EG@SiO_2 with 5,

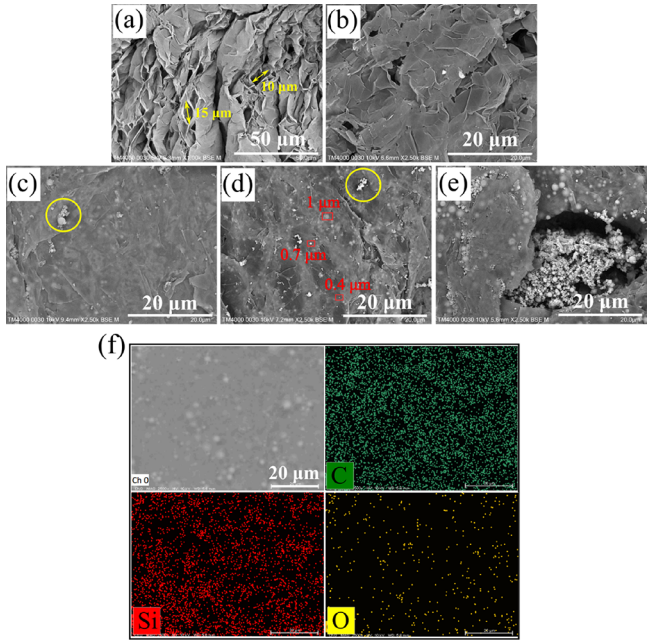

Figure 1. SEM images of (a, b) EG, (c−e) EG@SiO_2 with 5, 15, and 30 wt % SiO_2, and (f) EDS elemental mapping of EG@SiO_2 with 15 wt % SiO_2. The red rectangles in panel (d) highlight some SiO_2 particles used for the determination of the particle size.

15, and 30 wt % SiO_2. Pristine EG (Figure 1a,b) consisted of loosely layered graphite flakes, forming a porous network with macropores mainly below 15 μm in size. In the SEM images of EG@SiO_2 with 5, 15, and 30 wt % SiO_2 (Figure 1c−e), SiO_2 particles were deposited on the EG surfaces and clustered together some areas (marked by the yellow circle in Figure 1c,d) for the 5 and 15 wt % SiO_2 modified ones. The SiO_2 particles had sizes of about a submicrometer (0.4−1 μm), as seen in Figure 1d. However, when the SiO_2 content reached 30 wt %, a large number of unexpected clusters of SiO_2 were formed (Figure 1e), indicating an excess SiO_2 used at this rate. These excessive SiO_2 clusters were unnecessary because they did not attach to EG surfaces, while the excess SiO_2 amount resulted in a decrease in the fraction of EG in the prepared EG@SiO_2, negatively affecting the desired properties of this porous support type. The EDS elemental mapping of a representative EG@SiO_2 at 15 wt % SiO_2 (Figure 1f) presented sharp signals of Si and O eventually distributed on the EG surfaces, confirming the successful incorporation of SiO_2 onto the surfaces of EG.

Figure 2a,b compares the behaviors of pristine EG and a representative EG@SiO_2 with 15 wt % SiO_2 when they were added to melted PEG. The EG@SiO_2 readily adsorbed PEG and sank to the bottom after 15 min, while the pristine EG remained floating on the surface of the PEG. This observation indicates that the hydrophilicity of EG was improved by the presence of hydrophilic SiO_2, thus producing a good affinity to PEG. Figure 2c shows a significant enhancement of PEG

https://doi.org/10.1021/acsomega.3c04311
ACS Omega 2023, 8, 38160−38169

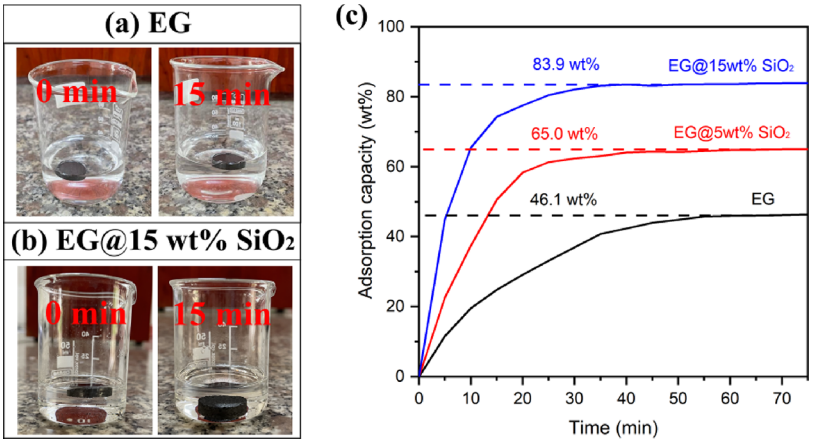

Figure 2. Digital photos of (a) EG and (b) EG@SiO_2 immersed into the melted PEG solution recorded at the beginning time and after 15 min, and (c) PEG adsorption capacity within the prisitne EG and EG@SiO_2 with 5 and 15 wt % SiO_2, respectively.

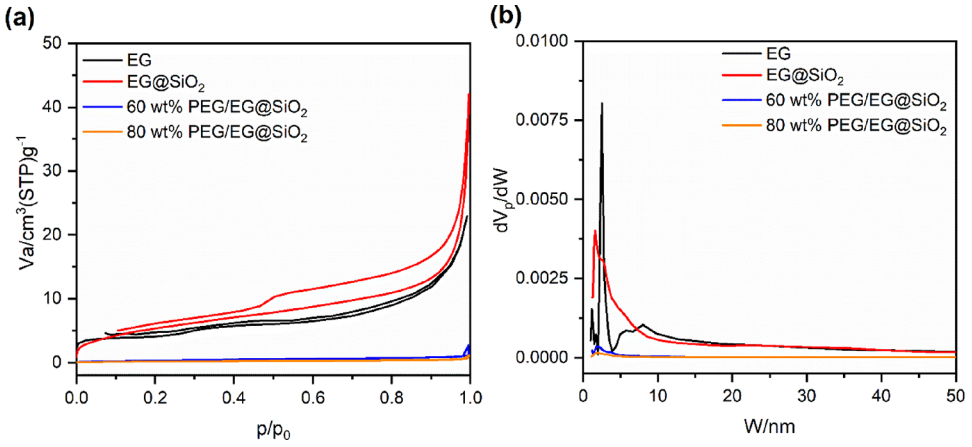

Figure 3. (a) N_2 adsorption−desorption isotherms of EG, EG@SiO_2, and two FSPCMs at 60 and 80 wt % PEG and (b) relevant pore size distribution. The curves of EG were obtained from our previous report.[22]

loading into SiO_2-modified EG compared to the pristine EG, including both adsorption capacity and rate. For instance, the saturated PEG content increased from 46.1 (in 60 min) to 65.0 (in 45 min) and 83.9 wt % (in 35 min) for the pristine E and EG@SiO_2 at 5 and 15% modified SiO_2, respectively. This suggests the hydrophilic compatibility of SiO_2-modified EG in the adsorption of PEG, allowing the effective preparation of PEG-based FSPCMs. The 15 wt % SiO_2 modified EG almost reached an optimum condition for loading PEG, and thus, it was selected as an optimal support, named EG@SiO_2, for further experiments.

The porosity properties of EG@SiO_2 compared to the pristine EG were investigated by N_2 adsorption−desorption isotherms, as shown in Figure 3. The detailed data are listed in Table 1. The EG@SiO_2 possessed enhanced porosities compared to pristine EG. The specific surface area of EG@SiO_2 was 33% higher than that of EG, possibly due to the contribution of deposited large surface area of SiO_2 nanoparticles. Although both EG and EG@SiO_2 presented mesopores within a wide range of 2−50 nm (Figure 3b), the pores of EG@SiO_2 were slightly enlarged to a range of 2−10 nm, while a range of 2−5 nm was observed for the EG pores. Consequently, the pore volume (V_p) of EG@SiO_2 was 85.7% greater than that of EG (Table 1). The SiO_2 submicroparticles could easily enter the EG macropores and deposit on surfaces, resulting in the increased specific surface area. In addition, new intergranular micromesopores could be formed for the deposited SiO_2 particles, making the pore size distribution enlarged, the pore volume increased, and the specific surface area as well.[16,21] The possibility of SiO_2 particles blocking mesopores (2−50 nm) of EG can be negligible (refer to the pore size distribution in Figure 3) and thus may not result in a decrease in the overall specific surface area and pore volume of the EG@SiO_2. Similar phenomena have been recently reported in the literature for EG modification with SiO_2 particles.[16,21] This indicates that the modification with SiO_2 can tune the surface and structural properties of EG, offering more space and interaction sites for shape-stabilizing PEG.

The PEG/EG@SiO_2 FSPCMs were prepared with varying PEG content ranging from 60 to 90 wt % (as described in Section 4.2), and their morphologies were presented by SEM

Table 1. Porosity Properties of EG, EG@SiO_2, and Two FSPCMs at 60 and 80 wt % PEG

	S (m^2/g)	V_p (cm^3/g)[a]
EG	15	0.035
EG@SiO_2	20	0.065
60 wt % PEG/EG@SiO_2		
80 wt % PEG/EG@SiO_2		

[a]V_p was calculated at a P/P_0 of 0.97.

https://doi.org/10.1021/acsomega.3c04311
ACS Omega 2023, 8, 38160−38169

images (Figure 4). As the PEG content increased, the porous networks of EG@SiO_2 in the FSPCMs were progressively filled. The N_2 adsorption−desorption isotherms of two representative FSPCMs at 60 and 80 wt % PEG (Figure 4a) showed declined N_2 uptake, consistent with the disappearance of pores in their corresponding pore size distribution (Figure 4b). These results indicated the successful impregnation of PEG into the EG@SiO_2. Notably, in the FSPCM with 90 wt % PEG, the surfaces of EG@SiO_2 were not visible possibly due to the coverage of PEG (Figure 3d), indicating an excessive amount of PEG in this composite. To confirm the PEG content in the prepared FSPCMs, the TGA analysis was performed to calculate the weight losses of PEG as the temperature increases (see later in Figure 7). As shown, the PEG contents were found to be 61.2, 70.8, 79.2, and 90.6 wt % corresponding to the 60, 70, 80, and 90 wt % loaded PEG, respectively. This indicates that PEG was evenly dispersed and efficiently infiltrated the porous network of the EG@SiO_2 host.

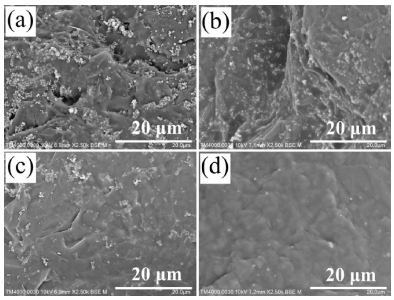

Figure 4. SEM images of PEG/EG@SiO_2 FSPCMs at PEG contents of (a) 60, (b) 70, (c) 80, and (d) 90 wt %.

Figure 5a shows the FTIR spectra of EG, EG@SiO_2, PEG, and the obtained PEG/EG@SiO_2 FSPCMs with 60 and 80 wt % PEG. The spectrum of EG exhibited characteristic peaks of the C=C vibration (1604 cm^{-1}) and −OH vibration (3425 cm^{-1}) of phenolic and/or alcoholic functional groups, respectively.[22] In the spectrum of EG@SiO_2, the characteristic absorption of EG merged with those of SiO_2. Specifically, the peak at 3442 cm^{-1} was attributed to the overlapped vibrations of surface silanol (Si−OH) groups from SiO_2 and the −OH groups from EG, while the bands at 1096, 802, and 465 cm^{-1} were related to the vibrations of Si−O−Si bonds,[23] indicating the successful incorporation of the two substances. The FTIR spectra of the representative PEG/EG@SiO_2 FSPCMs showed the combination of the inherent characteristics of the EG@SiO_2 host and PEG loading. For instance, the additional peaks inherited from PEG were observed for C−H vibrations at 2888, 1468, 1282, 957, and 841 cm^{-1}, respectively and C−O−C vibration at 1064 cm^{-1}.[24] The broad peak centered at approximately 3423 cm^{-1} originated assigned to the overlapped peaks of the Si−OH group from SiO_2 and the −OH groups from EG and PEG. Importantly, no new peak was found in the patterns of the FSPCMs, indicating that PEG and EG@SiO_2 were physically composited without chemical reactions.

Figure 5b displays the XRD patterns of the two representative FSPCMs containing 60 and 80 wt % PEG that present both the diffraction peaks of each PEG and EG@SiO_2. Specifically, the distinct diffractions at 2θ values of 19.2 and 23.4° corresponded well to the (120) and (032) crystal planes of PEG, respectively,[25,26] while the diffraction peak at 2θ of 26.6° corresponded to the characteristic (002) crystal plane of EG.[27] It is noted that no apparent diffraction of SiO_2 could be observed, because of its intrinsic amorphous nature. These results demonstrated that the crystallization nature of PEG was maintained as it was encapsulated in the porous network of EG@SiO_2.

2.2. Phase Change Characteristics of PEG/EG@SiO_2 FSPCMs. The high phase change efficiency of PEG/EG@SiO_2 FSPCMs is a prerequisite for their thermal energy storage performance. In this regard, the phase change characteristics were investigated by DSC analysis and are presented in Figure 6, and the detailed data of melting/crystallization temperature (T_M/T_C) is summarized in Table 2. A single−phase change model during melting and crystallization was observed for both the FSPCMs and pristine PEG although the FSPCMs underwent slightly reduction in both melting (1.0−3.9 °C) and crystallization (1.6−4.7 °C) temperatures with increasing PEG content. When PEG was encapsulated in EG@SiO_2 porous network, interactions (H-bonds, surface tension) occurring between PEG and EG@SiO_2 could affect the crystallization behaviors of PEG, thus decreasing the phase change temperature.[28,29] In addition, the phase change temperature reduction could also be attributed to strained PEG molecules as encapsulated in the mesopore structure of EG@SiO_2 (2−10 nm).[30]

Table 2 shows that pristine PEG had melting and crystallization enthalpies ($\Delta H_M/\Delta H_C$), which represent the thermal energy storage capacity, of 177.8 and 175.6 J/g, respectively. These values are in agreement with reported

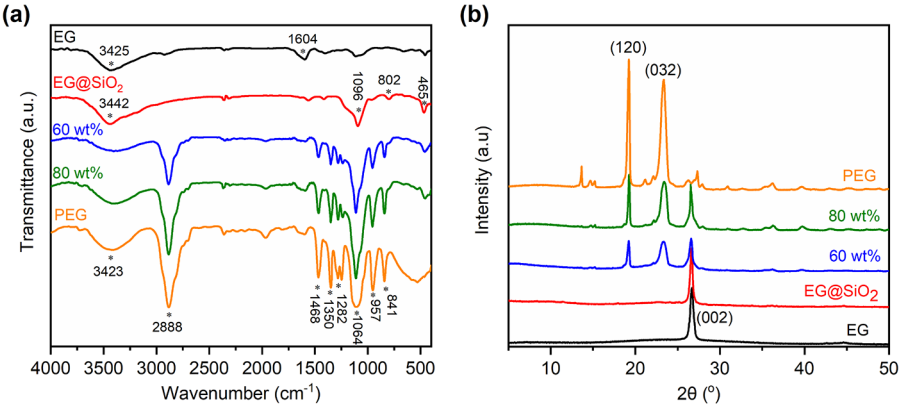

Figure 5. (a) FTIR patterns and (b) XRD spectra of EG, EG@SiO_2, PEG, and PEG/EG@SiO_2 FSPCMs at 60 and 80 wt % PEG.

https://doi.org/10.1021/acsomega.3c04311
ACS Omega 2023, 8, 38160−38169

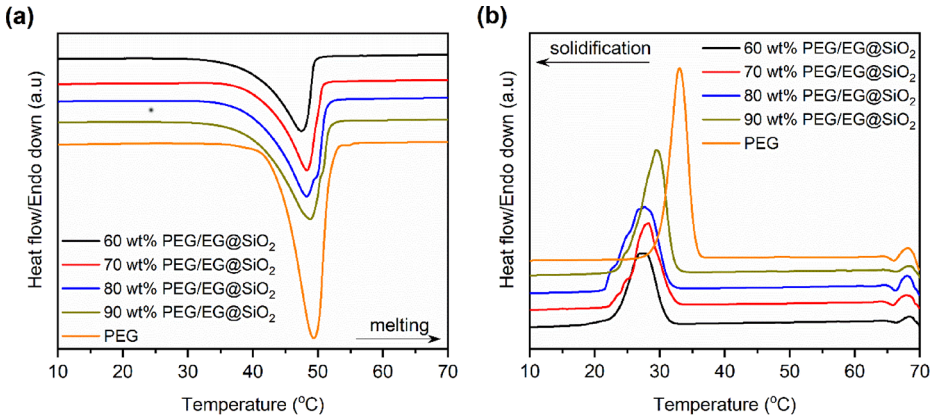

Figure 6. (a) Melting DSC thermograms of PEG and the obtained PEG/EG@SiO_2 FSPCMs and (b) crystallization DSC thermograms of PEG and the obtained PEG/EG@SiO_2 FSPCMs.

Table 2. Phase Transition Characteristics of PEG/EG@SiO_2 FSPCMs Compared to Pure PEG

	T_M (°C)	ΔH_M (J/g)	T_C (°C)	ΔH_C (J/g)	F (%)
60 wt %	37.9	91.5	30.7	91.3	85.8
70 wt %	39.5	110.5	32.2	109.8	88.8
80 wt %	39.7	132.5	32.0	131.9	93.2
90 wt %	39.8	153.9	33.8	152.3	96.2
PEG	41.8	177.8	35.4	175.6	100.0
80 wt % 500 cycles	39.5	131.8	31.9	130.1	92.6

values.[5,6] However, the obtained FSPCMs exhibited lower phase change enthalpies compared to pristine PEG. The ΔH_M values ranged from 91.5 to 153.9 J/g, and the ΔHC values ranged from 91.3 to 152.3 J/g as the PEG quantity increased from 60 to 90 wt %. This reduction in the phase change enthalpy could be explained by the inclusion of EG@SiO_2, which decreased the fraction of PEG available as the active heat storage material. As a result, increasing the PEG content in the FSPCMs led to a higher amount of latent heat absorption and desorption. Another possible reason is that at higher PEG contents, the factors that negatively affect the crystallinity of confined PEG could be alleviated. The crystallinity of PEG encapsulated in the FSPCMs can be estimated by computing the crystallization fraction (F (%)) using eq 1).[31,32]

$$F = \frac{\Delta H_{M,\mathrm{FSPCM}}}{\Delta H_{M,PCM} \cdot w} \times 100\% \quad (1)$$

where $\Delta H_{M,\mathrm{FSPCM}}$ and $\Delta H_{C,\mathrm{FSPCM}}$ are the ΔH_M and ΔH_C values of PEG/EG@SiO_2 FSPCMs, respectively; $\Delta H_{M,\mathrm{PEG}}$ and $\Delta H_{C,\mathrm{PEG}}$ are the ΔH_M and ΔH_C values of the pristine PEG, respectively, and w_{PEG} is the mass fraction of PEG in the FSPCM. The obtained F values in Table 2, which represent the crystallinity of confined PEG, were all below 100% and increased from 85.8 to 96.2% as the PEG quantity increased from 60 to 90 wt %, respectively. This indicates that the crystallinity of PEG was more strongly impeded when a smaller fraction of PEG was incorporated with EG@SiO_2. In the FSPCM, when PEG came into direct contact with the surfaces of EG@SiO_2, it was likely to hydrogen−bond with surface silanol from SiO_2 and phenolic and alcoholic functional groups from EG.[22,33] These H−bonds restricted the ordered array of PEG chains during crystallization, thereby reducing the crystallization fraction.[34−36] When PEG was impregnated into the porous network of EG@SiO_2 at lower contents, most of the PEG was adsorbed onto the surfaces of EG@SiO_2 and formed H−bond interactions. As a result, the crystallization fraction was low. However, once the surfaces of EG@SiO_2 were fully covered with PEG, the sublayer of PEG during additional infiltration does not come into contact with the surfaces and is free from H−bonds. Consequently, the crystallization efficiency of confined PEG was enhanced at higher PEG quantities.

2.3. Thermal Stability and Leakage−Proof Ability of PEG/EG@SiO_2 FSPCMs. The thermal stability of the PEG/EG@SiO_2 FSPCMs, compared to that of pristine PEG, was characterized by TGA as shown in Figure 7. Pristine PEG

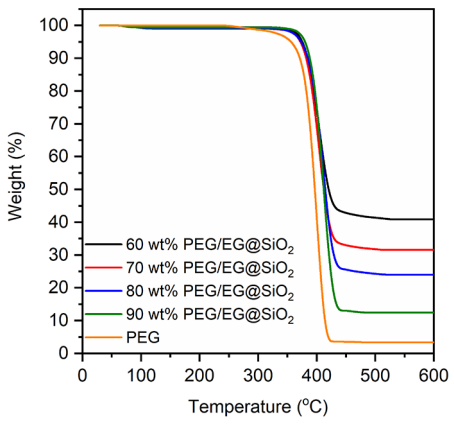

Figure 7. TGA curves of PEG and the obtained PEG/EG@SiO_2 FSPCMs. The TGA curve of pure PEG was obtained from our recent report.[25]

showed a one−step degradation within a temperature range of 370−417 °C. The obtained PEG/EG@SiO_2 FSPCMs also underwent one−step thermal decomposition but with a slightly higher decomposition temperature range of 382−433 °C. As confined in the EG@SiO_2 porous network, PEG can be restricted by interactions with the porous host such as H-bonds, surface tension, and capillary forces, limiting its movement and overflow. Consequently, the thermal stability of the FSPCMs was enhanced. This suggests that the obtained FSPCMs can exhibit high thermal stability during the storage/release operations because the thermal decomposition temperature was significantly higher than the heat storage/release

https://doi.org/10.1021/acsomega.3c04311
ACS Omega 2023, 8, 38160−38169

phase change temperature (~40 °C). The high thermal stability could allow the FSPCMs used in a wide range of temperature conditions.

The leakage−proof ability of the PEG/EG@SiO_2 composites, compared to that of pristine PEG, was evaluated after thermal treatment at 60 °C (16 °C greater than the melting point of PEG), as shown in Figure 8. The poor leakage-proof

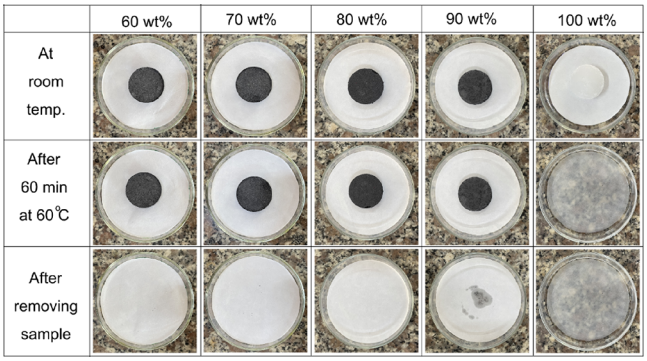

Figure 8. Photographs of PEG and the obtained PEG/EG@SiO_2 FSPCMs during the anti−leakage test.

ability of pure PEG was overcome in the obtained FSPCMs with PEG contents of 60−80 wt % that exhibited good leakage−proof ability without any observed leakage and maintained their primary shapes. In addition to the surface tension and capillary force, the introduction of SiO_2 onto EG surfaces could promote a good affinity to PEG and form strongly interfacial H-bonds between PEG and SiO_2 surfaces, effectively resisting shape deformation and leakage of the melted PEG, resulting in excellent stability of the prepared FSPCMs. However, the FSPCM with 90 wt % PEG showed slight leakage despite maintaining a stable form. This can be attributed to excessive PEG on the surfaces of EG@SiO_2, as seen in Figure 4d. The excessive PEG had insufficient interactions with the porous matrix, leading to some leakage.

2.4. Thermal Conductivity and Heat Storage/Release of PEG/EG@SiO_2 FSPCMs. Figure 9a compares the thermal conductivity of the obtained PEG/EG@SiO_2 FSPCMs to pristine PEG. The poor thermal conductivity of pristine PEG (0.286 W/m·K) was dramatically enhanced in the form of FSPCMs (2.852−7.126 W/m·K) with a factor range of 10.0−24.7 times. The EG@SiO_2 with interconnected porous networks could offer effectively thermally conductive scaffolds for producing thermal paths and increasing the surface area of PEG. Furthermore, the ultrahigh thermal conductivity of EG also contributed to boosting the overall thermal conductivity of the FSPCMs, with the thermal conductivity increasing with higher EG content. Previous studies have reported that FSPCMs with 6−15 wt % EG exhibited thermal conductivities 7.16−17.3 times superior over those of pure PCMs.[37−39] The high thermal conductivity of PEG/EG@SiO_2 FSPCMs could promote fast heat transfer during heat storage and release processes. Indeed, in Figure 9b, it can be seen that the 80 wt % PEG/EG@SiO_2 FSPCM achieved rapid heat storage and release, taking only 180 and 90 s, respectively. In contrast, pristine PEG required significantly longer times, with heat storage and release taking up to 2470 and 820 s, respectively. The 80 wt % PEG/EG@SiO_2 FSPCM exhibited heat storage and release rates that were 13.7 and 9.1 times faster, respectively, compared to pristine PEG. This enhanced thermal performance is due to the great thermal conductivity of the FSPCM, which allows for efficient heat transfer and faster heat storage and release processes.

Overall, the obtained 80 wt % PEG/EG@SiO_2 FSPCM presented high heat storage capacity and thermal conductivity, which can be comparable to or even better than other PEG−based FSPCMs recently reported (Table 3). The FSPCMs including PEG/$SrBaCO_3$, PEG/biomass, and PEG/BPC−Ag porous carbon presented high thermal energy storage capacities but low thermal conductivities. Meanwhile, the other FSPCMs including PEG/mRHA, PEG/SiO_2, PEG/mesoporous SiO_2, and PEG/mica presented low thermal energy storage capacities as well as low thermal conductivities.

2.5. Cycling durability of PEG/EG@SiO_2 FSPCM. The cycling durability of the 80 wt % PEG/EG@SiO_2 FSPCM was evaluated through 500 melting/crystallization cycles. Figure 10(a) shows a negligible change of DSC curves compared before and after the 500th thermal cycles, where the T_M and ΔH_M decreased only 0.2 °C and 0.5% after the operations, respectively (Table 2). This indicates the excellent stability of the thermal characteristics of the FSPCM even after undergoing multiple cycles of heat transfer. Furthermore, the FTIR spectra of the FSPCM before and after the 500th cycle test (Figure 10(b)) show no apparent change in the relative intensity and frequency of vibration peaks, indicating the chemical structure of the FSPCM remained intact after the multiple phase change processes.

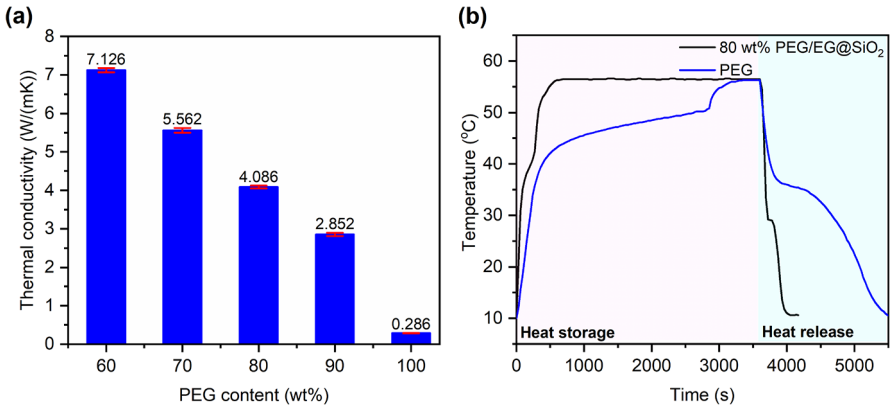

Figure 9. (a) Thermal conductivities of PEG and the obtained PEG/EG@SiO_2 FSPCMs and (b) heat storage and release properties of PEG and the obtained 80 wt % PEG/EG@SiO_2 FSPCM.

https://doi.org/10.1021/acsomega.3c04311
ACS Omega 2023, 8, 38160−38169

Table 3. Thermal Properties of the 80 wt % PEG/EG@SiO_2 FSPCM Compared to Those of Other FSPCMs

FSPCMs	pptimum PCM content (wt %)	ΔH_M (J/g)	thermal conductivity (W/m·K)	ref
PEG/mRHA	63.6	119.3	0.3197	40
PEG/ mesoporous SiO_2	90	133.7	not available	28
PEG/$SrBaCO_3$	71.5	148.8	0.298	6
PEG/biomass porous carbon	86.3	152.9	not available	5
PEG/diatom−based biomass	71.5	121.54	not available	41
PEG/SiO_2	80	132.4	0.33	29
PEG/ mesoporous SiO_2	70	88.2	not available	7
PEG/ mesoporous SiO_2	60	58.76	not available	8
PEG/mica	46.2	77.75	not available	42
PEG/BPC−Ag	81.4	140.3	0.639	43
PEG/EG@SiO_2	80	132.5	4.086	this work

3. CONCLUSION

The fabrication of PEG/EG@SiO_2 FSPCMs has been successfully achieved, demonstrating excellent polar compatibility and a high thermal performance. The EG@SiO_2 carrier was prepared by using a simple and cost−effective sol−gel method, utilizing sodium silicate as the SiO_2 precursor. The deposition of SiO_2 particles onto the surfaces of EG resulted in good hydrophilicity, enabling effective incorporation with PEG. The prepared PEG/EG@SiO_2 FSPCMs exhibited melting temperatures ranging from 37.9 to 39.8 °C and thermal energy storage capacities ranging from 91.5 to 153.9 J/g with increasing PCM content from 60 to 90 wt %. The crystallinity of the encapsulated PEG increased with higher PEG quantities, and a high crystallinity of 93.5% was achieved when 80 wt % of PEG was stabilized in the EG@SiO_2 porous network. The thermal conductivities of the PEG/EG@SiO_2 FSPCMs ranged from 2.852 to 7.126 W/(m·K), which were significantly higher (10.0−24.7 times) than that of pure PEG. This enhanced thermal conductivity facilitated efficient heat transfer during the operation of the FSPCMs. The optimized FSPCM with 80 wt % PEG demonstrated heat storage and release rates that were respectively 13.7 and 9.1 times faster than pure PEG. Furthermore, a test involving multiple accelerated thermal cycles confirmed the excellent cycling durability of the FSPCM. The thermal properties of the FSPCM remained largely unchanged, with only a slight decrease in melting temperature and melting enthalpy observed after 500 cycles. Given their favorable thermal properties and cost−effectiveness, the prepared PEG/EG@SiO_2 FSPCMs hold great promise for large−scale thermal energy storage applications.

4. MATERIALS AND METHODS

4.1. Materials. Sodium silicate solution (26.5% SiO_2 and 10.6% Na_2O) and expandable graphite were purchased from Sigma−Aldrich (US). Acetic acid and ethanol were purchased from Xilong Chemical (China). PEG with a molecular weight of 1000 was obtained from Shanghai Zhangyun Chemical (China).

4.2. Preparation of PEG/EG@SiO_2 FSPCMs. First, expandable graphite was thermally treated at 800 °C for 1 min to result in EG. The obtained EG was further thermally treated at 350 °C for 4 h to convert the unsaturated C−C and ketone bonds to hydrophilic carboxyl groups.[16] The preparation process of EG@SiO_2 and PEG/EG@SiO_2 FSPCMs was illustrated in Figure 11. To 150 mL of a mixture of H_2O and ethanol (70:30 v/v), predetermined amounts of EG and sodium silicate solution were added to get a total mass of EG

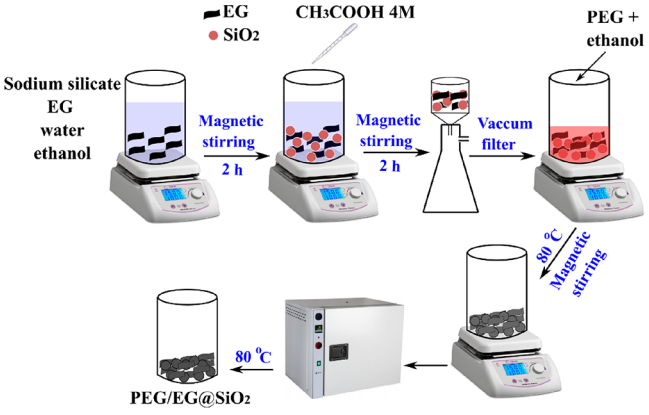

Figure 11. Preparation process of PEG/EG@SiO_2 FSPCMs.

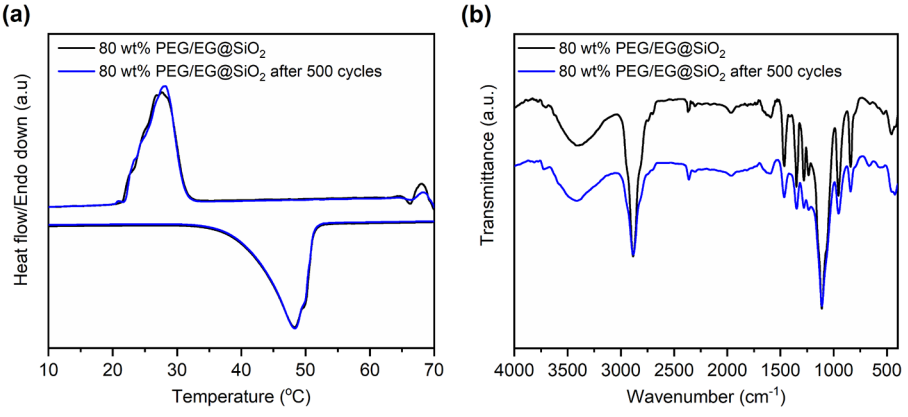

Figure 10. (a) DSC curves and (b) FTIR spectra of the obtained 80 wt % PEG/EG@SiO_2 FSPCMs before and after 500 melting/crystallization cycles.

https://doi.org/10.1021/acsomega.3c04311
ACS Omega 2023, 8, 38160−38169

and SiO_2 of 1g and mixed under magnetic stirring for 2 h. Acetic acid (4 M) was dropwise added until a pH value of ~4.5 was reached for the SiO_2 to precipitate, and the mixture was kept stirring at ambient temperature for 1 h. EG@SiO_2 was collected by the filter at low pressure, followed by calcination at 400 °C for 5 h. By changing the EG:SiO_2 ratio, three EG@SiO_2 materials with SiO_2 content of 5, 15, and 30 wt % were produced.

Subsequently, for the preparation of PEG/EG@SiO_2, a predetermined amount of PEG and approximately 2−3 mL of ethanol was introduced to the EG@SiO_2 with 15 wt % SiO_2 and the obtained blend was mixed at room temperature for 2 h for PEG to evenly disperse within the EG@SiO_2. The blend was heated at 80 °C for 24 h to remove the solvent and allow PEG to impregnate the EG@SiO_2 porous network. Different amounts of PEG were used to produce PEG/EG@SiO_2 FSPCMs with varying PEG quantities. The specific contents of PEG, EG, and SiO_2 in the prepared composites are presented in Table 4. As the PEG content increased, the contents of EG and SiO_2 correspondingly decreased.

Table 4. Contents of EG, SiO_2, and PEG in prepared PEG/EG@SiO_2 FSPCMs

FSPCMs	EG content (wt%)	SiO_2 content (wt%)	PEG content (wt%)
60 wt % PEG/EG@SiO_2	34	6	60
70 wt % PEG/EG@SiO_2	25.5	4.5	70
80 wt % PEG/EG@SiO_2	17	3	80
90 wt % PEG/EG@SiO_2	8.5	1.5	90

4.3. Characterization methods. Scanning electron microscopy (SEM) images and energy dispersive X-ray (EDS) elemental mapping were captured with a TM4000 system (Hitachi, Japan). The polar compatibility between PEG and porous carriers was checked by adding pristine EG and EG@SiO_2 into melted PEG and observing the adsorption after 15 min. The PEG adsorption capacity was evaluated by adding compressed samples of pristine EG and EG@SiO_2 into melted PEG. After every 5 min, the materials were taken out of the melted PEG and put onto filter papers to adsorb the PEG bound on the external surfaces of the materials. The loaded PEG amount was determined by weighing. The N_2 adsorption−desorption isotherm was recorded with a Micro-Active TriStar II Plus system (Micrometrics, US). The surface area and pore size distribution were computed by the Brunauer−Emmett−Teller (BET) and the Barrett, Joyner and Halenda methods, respectively. Fourier−transformed infrared spectroscopy (FTIR) spectra were collected using an FTIR 4600 spectrometer (Jasco, Japan). X−ray diffraction (XRD) patterns were recorded using an Empyrean diffractometer ((Malvern, UK) with Cu Kα radiation between 2θ range of 5−50°. The thermophysical properties were analyzed by a differential scanning calorimeter (DSC 214 Polyma, Netzsch, USA). The specimens were heated and cooled between 10 and 70 °C at a scanning speed of 5 °C/min under a nitrogen atmosphere. Thermogravimetric analysis (TGA) curves were collected using a Labsys Evo TG−DSC 1600 system (Setaram, US) within 30−600 °C at a scanning speed of 10 °C/min under a inert gas. The thermal conductivities were obtained using a TPS 3500 system (Hot Disk AB, Sweden).

The leakage resistance was tested by placing round blocks (30 mm × 10 mm) of materials on filtered papers and isothermally treating them for 60 min at 60 °C. Subsequently, the round blocks were separated, and the leakage was determined by observing the filter papers. The cycling durability was measured by repeatedly shifting the samples between two baths at 0 and 60 °C for 500 cycles with the duration at each bath of 5 min.

The heat storage and release properties were studied by measuring temperature−time curves of materials as they were heated and cooled using an experimental apparatus developed in our recent report.[25] In brief, a material (25 g) was packed into a cylinder (30 mm × 70 mm), preconditioned in a bath at 10 °C and then moved to another bath at 60 °C for melting. When a stable temperature was reached, the material was moved to the bath at 10 °C for crystallization. The temperature change of the material during the heating and cooling was recorded using a thermocouple (Ika ETS−D5).

AUTHOR INFORMATION

Corresponding Author

Giang Tien Nguyen − *Faculty of Chemical and Food Technology, Ho Chi Minh City University of Technology and Education (HCMUTE), Ho Chi Minh City 700000, Vietnam;* orcid.org/0000-0003-0216-2735; Email: ntgiang@hcmute.edu.vn

Authors

Thi Ai Nhi Truong − *Faculty of Chemical and Food Technology, Ho Chi Minh City University of Technology and Education (HCMUTE), Ho Chi Minh City 700000, Vietnam*

Nguyen Duy Dat − *Faculty of Chemical and Food Technology, Ho Chi Minh City University of Technology and Education (HCMUTE), Ho Chi Minh City 700000, Vietnam*

Thi Anh Dao Phan − *Faculty of Chemical and Food Technology, Ho Chi Minh City University of Technology and Education (HCMUTE), Ho Chi Minh City 700000, Vietnam*

Trung Huu Bui − *Faculty of Chemical and Food Technology, Ho Chi Minh City University of Technology and Education (HCMUTE), Ho Chi Minh City 700000, Vietnam; The Connecticut Agricultural Experiment Station, New Haven, Connecticut 06511, United States*

Complete contact information is available at: https://pubs.acs.org/10.1021/acsomega.3c04311

Notes

The authors declare no competing financial interest.

ACKNOWLEDGMENTS

The research topic was supported by The Youth Incubator for Science and Technology Programme, managed by Youth Promotion Science and Technology Center - Ho Chi Minh Communist Youth Union and Department of Science and Technology of Ho Chi Minh City, the contract number is 43/2022/HĐ-KHCNT-VU" signed on 30 th, December, 2022.

https://doi.org/10.1021/acsomega.3c04311
ACS Omega 2023, 8, 38160−38169

REFERENCES

(1) Eanest Jebasingh, B.; Valan Arasu, A. A comprehensive review on latent heat and thermal conductivity of nanoparticle dispersed phase change material for low-temperature applications. *Energy Stor. Mater.* **2020**, *24*, 52−74.

(2) Naveenkumar, R.; Ravichandran, M.; Mohanavel, V.; Karthick, A.; Aswin, L. S. R. L.; Priyanka, S. S. H.; Kumar, S. K.; Kumar, S. P. Review on phase change materials for solar energy storage applications. *Environ. Sci. Pollut. Res.* **2022**, *29* (7), 9491−9532.

(3) Rathore, P. K. S.; Shukla, S. K. Enhanced thermophysical properties of organic PCM through shape stabilization for thermal energy storage in buildings: A state of the art review. *Energy Build.* **2021**, *236*, No. 110799.

(4) Prajapati, D. G.; Kandasubramanian, B. A Review on Polymeric-Based Phase Change Material for Thermo-Regulating Fabric Application. *Polym. Rev.* **2020**, *60* (3), 389−419.

(5) Zhou, K.; Sheng, Y.; Guo, W.; Wu, L.; Wu, H.; Hu, X.; Xu, Y.; Li, Y.; Ge, M.; Du, Y.; Lu, X.; Qu, J. Biomass porous carbon/polyethylene glycol shape-stable phase change composites for multi-source driven thermal energy conversion and storage. *Adv. Compos. Hybrid Mater.* **2023**, *6* (1), 34.

(6) Mohaisen, K. O.; Zahir, M. H.; Maslehuddin, M. Shape-stabilized phase change material for thermal energy storage: Sr^{+2} doped $BaCO_3$ matrix incorporating polyethylene glycol. *J. Energy Storage* **2023**, *58*, No. 106369.

(7) Wang, J.; Yang, M.; Lu, Y.; Jin, Z.; Tan, L.; Gao, H.; Fan, S.; Dong, W.; Wang, G. Surface functionalization engineering driven crystallization behavior of polyethylene glycol confined in mesoporous silica for shape-stabilized phase change materials. *Nano Energy* **2016**, *19*, 78−87.

(8) Feng, D.; Feng, Y.; Li, P.; Zang, Y.; Wang, C.; Zhang, X. Modified mesoporous silica filled with PEG as a shape-stabilized phase change materials for improved thermal energy storage performance. *Microporous Mesoporous Mater.* **2020**, *292*, No. 109756.

(9) Karaman, S.; Karaipekli, A.; Sarı, A.; Biçer, A. Polyethylene glycol (PEG)/diatomite composite as a novel form-stable phase change material for thermal energy storage. *Sol. Energy Mater. Sol. Cells* **2011**, *95* (7), 1647−1653.

(10) Feng, L.; Zhao, W.; Zheng, J.; Frisco, S.; Song, P.; Li, X. The shape-stabilized phase change materials composed of polyethylene glycol and various mesoporous matrices (AC, SBA-15 and MCM-41). *Sol. Energy Mater. Sol. Cells* **2011**, *95* (12), 3550−3556.

(11) Ao, C.; Yan, S.; Zhao, S.; Hu, W.; Zhao, L.; Wu, Y. Stearic acid/expanded graphite composite phase change material with high thermal conductivity for thermal energy storage. *Energy Rep.* **2022**, *8*, 4834−4843.

(12) Li, C.; Zhang, B.; Liu, Q. N-eicosane/expanded graphite as composite phase change materials for electro-driven thermal energy storage. *J. Energy Storage* **2020**, *29*, No. 101339.

(13) Zeng, J.-L.; Gan, J.; Zhu, F.-R.; Yu, S.-B.; Xiao, Z.-L.; Yan, W.-P.; Zhu, L.; Liu, Z.-Q.; Sun, L.-X.; Cao, Z. Tetradecanol/expanded graphite composite form-stable phase change material for thermal energy storage. *Sol. Energy Mater. Sol. Cells* **2014**, *127*, 122−128.

(14) Liu, S.; Zhang, X.; Zhu, X.; Xin, S. A Low-Temperature Phase Change Material Based on Capric-Stearic Acid/Expanded Graphite for Thermal Energy Storage. *ACS Omega* **2021**, *6* (28), 17988−17998.

(15) Zhao, Y.; Jin, L.; Zou, B.; Qiao, G.; Zhang, T.; Cong, L.; Jiang, F.; Li, C.; Huang, Y.; Ding, Y. Expanded graphite − Paraffin composite phase change materials: Effect of particle size on the composite structure and properties. *Appl. Therm. Eng.* **2020**, *171*, No. 115015.

(16) Chen, W.; Liang, X.; Wang, S.; Ding, Y.; Gao, X.; Zhang, Z.; Fang, Y. SiO_2 hydrophilic modification of expanded graphite to fabricate form-stable ternary nitrate composite room temperature phase change material for thermal energy storage. *Chem. Eng. J.* **2021**, *413*, No. 127549.

(17) Duan, Z.-j.; Zhang, H.-z.; Sun, L.-x.; Cao, Z.; Xu, F.; Zou, Y.-j.; Chu, H.-l.; Qiu, S.-j.; Xiang, C.-l.; Zhou, H.-y. $CaCl_2{\cdot}6H_2O$/Expanded graphite composite as form-stable phase change materials for thermal energy storage. *J. Therm. Anal. Calorim.* **2014**, *115* (1), 111−117.

(18) Zhou, Y.; Sun, W.; Ling, Z.; Fang, X.; Zhang, Z. Hydrophilic Modification of Expanded Graphite to Prepare a High-Performance Composite Phase Change Block Containing a Hydrate Salt. *Ind. Eng. Chem. Res.* **2017**, *56* (50), 14799−14806.

(19) Zou, T.; Fu, W.; Liang, X.; Wang, S.; Gao, X.; Zhang, Z.; Fang, Y. Hydrophilic modification of expanded graphite to develop form-stable composite phase change material based on modified $CaCl_2{\cdot}6H_2O$. *Energy* **2020**, *190*, No. 116473.

(20) Gong, S.; Cheng, X.; Li, Y.; Shi, D.; Wang, X.; Zhong, H. Enhancement of ceramic foam modified hierarchical Al_2O_3@expanded graphite on thermal properties of 1-octadecanol phase change materials. *J. Energy Storage* **2019**, *26*, No. 101025.

(21) Fang, Y.; Diao, W.; Su, J.; Liang, X.; Wang, S.; Gao, X.; Zhang, Z. Preparation and thermal performances of $Na_2HPO_4{\cdot}12H_2O/SiO_2$ hydrophilic modified expanded graphite form-stable composite phase change material for radiant floor heating system. *Sol. Energy Mater. Sol. Cells* **2021**, *230*, No. 111221.

(22) Nguyen, G. T.; Ly, T. N.; Tran, N. T.; Tuan, H. N. A.; Hieu, N. H.; Bui, T. H. Glutaric acid/expanded graphite composites as highly efficient shape-stabilized phase change materials at medium-temperature. *J. Energy Storage* **2023**, *63*, No. 107038.

(23) Nguyen, G. T.; Do, M. H.; Ly, T. N.; Park, I.; Bui, T. H. Novel shape-stabilized phase change materials: Insights into the thermal energy storage of 1-octadecanol/fumed silica composites. *J. Energy Storage* **2022**, *52*, No. 104772.

(24) Chen, Y.; Ding, H.; Wang, B.; Shi, Q.; Gao, J.; Cui, Z.; Wan, Y. Dopamine functionalization for improving crystallization behaviour of polyethylene glycol in shape-stable phase change material with silica fume as the matrix. *J. Cleaner Prod.* **2019**, *208*, 951−959.

(25) Nguyen, G. T. Polyethylene glycol/fumed silica composites as shape-stabilized phase change materials with effective thermal energy storage. *RSC Adv.* **2023**, *13* (11), 7621−7631.

(26) Wu, Y.; Li, L.; Chen, S.; Qin, J.; Chen, X.; Zhou, D.; Wu, H. Synthesis, characterization, and crystallization behaviors of poly(D-lactic acid)-based triblock copolymer. *Sci Rep* **2020**, *10* (1), 3627.

(27) Wang, T.; Liu, Y.; Meng, R.; Zhang, M. Thermal performance of galactitol/mannitol eutectic mixture/expanded graphite composite as phase change material for thermal energy harvesting. *J. Energy Storage* **2021**, *34*, No. 101997.

(28) Feng, L.; Yu, R.; Li, Y.; Huang, Y.; Zhao, L. Shape−stabilized phase change materials composed of polyethylene glycol and ordered mesoporous silica synthesized from fly ash. *Thermochim. Acta* **2023**, *720*, No. 179428.

(29) Sun, K.; Kou, Y.; Zheng, H.; Liu, X.; Tan, Z.; Shi, Q. Using silicagel industrial wastes to synthesize polyethylene glycol/silica-hydroxyl form-stable phase change materials for thermal energy storage applications. *Sol. Energy Mater. Sol. Cells* **2018**, *178*, 139−145.

(30) Nomura, T.; Zhu, C.; Sheng, N.; Tabuchi, K.; Sagara, A.; Akiyama, T. Shape-stabilized phase change composite by impregnation of octadecane into mesoporous SiO_2. *Sol. Energy Mater. Sol. Cells* **2015**, *143*, 424−429.

(31) Gao, H.; Wang, J.; Chen, X.; Wang, G.; Huang, X.; Li, A.; Dong, W. Nanoconfinement effects on thermal properties of nanoporous shape-stabilized composite PCMs: A review. *Nano Energy* **2018**, *53*, 769−797.

(32) Tang, J.; Yang, M.; Yu, F.; Chen, X.; Tan, L.; Wang, G. 1-Octadecanol@hierarchical porous polymer composite as a novel shape-stability phase change material for latent heat thermal energy storage. *Appl. Energy* **2017**, *187*, 514−522.

(33) Qian, T.; Li, J.; Ma, H.; Yang, J. The preparation of a green shape-stabilized composite phase change material of polyethylene glycol/SiO_2 with enhanced thermal performance based on oil shale ash via temperature-assisted sol−gel method. *Sol. Energy Mater. Sol. Cells* **2015**, *132*, 29−39.

(34) Nguyen, G. T.; Anh Tuan, H. N.; Park, I. Shape-Stabilized Phase Change Materials of Stearic Acid Confined in Fumed Silica. *Energy Fuels* **2022**, *36* (21), 13337−13345.

https://doi.org/10.1021/acsomega.3c04311
ACS Omega 2023, 8, 38160−38169

(35) Li, B.; Shu, D.; Wang, R.; Zhai, L.; Chai, Y.; Lan, Y.; Cao, H.; Zou, C. Polyethylene glycol/silica (PEG@SiO_2) composite inspired by the synthesis of mesoporous materials as shape-stabilized phase change material for energy storage. *Renewable Energy* **2020**, *145*, 84−92.
(36) Aftab, W.; Huang, X.; Wu, W.; Liang, Z.; Mahmood, A.; Zou, R. Nanoconfined phase change materials for thermal energy applications. *Energy Environ. Sci.* **2018**, *11* (6), 1392−1424.
(37) Li, F.; Zhen, H.; Li, L.; Li, Y.; Wang, Q.; Cheng, X. A template-method synthesis of mesoporous-MgO/expanded graphite for enhancing thermal properties of methyl palmitate-lauric acid phase change materials. *Mater. Today Energy* **2022**, *26*, No. 100999.
(38) Yuan, M.; Ren, Y.; Xu, C.; Ye, F.; Du, X. Characterization and stability study of a form-stable erythritol/expanded graphite composite phase change material for thermal energy storage. *Renewable Energy* **2019**, *136*, 211−222.
(39) Nguyen, G. T.; Hwang, H. S.; Lee, J.; Park, I. Azelaic Acid/Expanded Graphite Composites with High Latent Heat Storage Capacity and Thermal Conductivity at Medium Temperature. *ACS Omega* **2021**, *6* (12), 8469−8476.
(40) Yu, K.; Liu, Y.; Yang, Y. Enhanced thermal properties of polyethylene glycol/modified rice husk ash eco-friendly form-stable phase change material via optimizing support pore structure. *J. Energy Storage* **2021**, *43*, No. 103172.
(41) Huang, J.; Wu, B.; Lyu, S.; Li, T.; Han, H.; Li, D.; Wang, J.-K.; Zhang, J.; Lu, X.; Sun, D. Improving the thermal energy storage capability of diatom-based biomass/polyethylene glycol composites phase change materials by artificial culture methods. *Sol. Energy Mater. Sol. Cells* **2021**, *219*, No. 110797.
(42) Zhang, D.; Li, C.; Lin, N.; Xie, B.; Chen, J. Mica-stabilized polyethylene glycol composite phase change materials for thermal energy storage. *Int. J. Miner. Metall.* **2022**, *29* (1), 168−176.
(43) Xiao, S.; Zou, M.; Xie, Y.; Chen, W.; Hu, X.; Ma, Y.; Zu, S.; Che, Y.; Jiang, X. Nanosilver modified navel orange peel foam/polyethylene glycol composite phase change materials with improved thermal conductivity and photo-thermal conversion efficiency. *J. Energy Storage* **2022**, *56*, No. 105976.

https://doi.org/10.1021/acsomega.3c04311
ACS Omega 2023, 8, 38160−38169